

TABLE OF CONTENTS

	Page
Acknowledgments	iii
English Abstract	v
Thai Abstract	vii
List of Table	xiv
List of Figures	xvi
Abbreviations and symbols	xxiv
Chapter 1 Introduction	1
1.1 Principles, theory, rationale and/or hypotheses	1
1.2 Basic properties of research materials	2
1.2.1 Copper (II) oxide	2
1.2.2 Crystal structure and lattice parameters and mechanical properties of CuO	4
1.2.3 Zinc oxide	6
1.2.4 Crystal structure and lattices parameter and mechanical properties of ZnO	6
1.3 Motivation of research	8
1.4 Research objectives and usefulness	9
1.4.1 Objective	9
1.4.2 Usefulness	9

Chapter 2 CuO nanostructures	10
2.1 Literature review of preparation of CuO nanostructure	10
2.2 Preparation of CuO nanostructure	17
2.2.1 CuO nanowires by oxidation of copper plate	17
2.2.2 CuO nanowires by oxidation of copper powder	18
2.2.3 CuO thin films by oxidation of copper thin films	18
2.3 Properties of CuO nanostructures	19
2.3.1 CuO nanowires by oxidation of copper plate	19
2.3.1.1 FE-SEM of CuO nanowires by oxidation of copper plate	19
2.3.1.2 EDS result of CuO nanowires by oxidation of copper plate	22
2.3.1.3 TEM result of CuO nanowires by oxidation of copper plate	27
2.3.1.4 Raman spectra result of CuO nanowires by oxidation of copper plate	28
2.3.2 CuO nanowires by oxidation reaction of copper powder	29
2.3.2.1 FE-SEM of CuO nanowires by oxidation of copper powder	29
2.3.3 Growth mechanism of metal-oxide nanowire	30
2.3.4 CuO thin films by oxidation of thermal evaporated copper thin films	34
2.3.4.1 FE-SEM result of CuO thin films by thermal evaporated copper thin films	34

2.3.4.2 EDS result of CuO thin films by thermal evaporated copper thin films	36
2.3.4.3 XRD result of CuO thin films by thermal evaporated copper thin films	37
2.3.4.4 Raman spectra result of CuO thin films by thermal evaporation of copper thin films	38
Chapter 3 Copper oxide for ethanol sensor application	39
3.1 Literature review of CuO gas sensor	40
3.2 Ethanol sensing properties of CuO nanowires	45
3.2.1 Preparation of CuO nanowires for ethanol sensing	45
3.2.2 Experimental system for ethanol sensing properties	46
3.2.3 Ethanol sensing result for CuO nanowires	48
Chapter 4 Copper oxide nanostructure for dye-sensitized solar cell application	52
4.1 Literature review of CuO nanostructures for dye-sensitized solar cell applications	54
4.1.1 CuO nanostructures as a cathode in dye-sensitized solar cells	54
4.1.2 p-n junction device of CuO in application of photodevice	56
4.1.3 p-n junction DSSC	58
4.1.4 CuO as photoelectrode in DSSCs	61
4.1.5 Passivating layer for improving efficiency of DSSCs	63
4.2 Experimental of dye-sensitized solar cell applications	65
4.2.1 Solar cells measurement	65

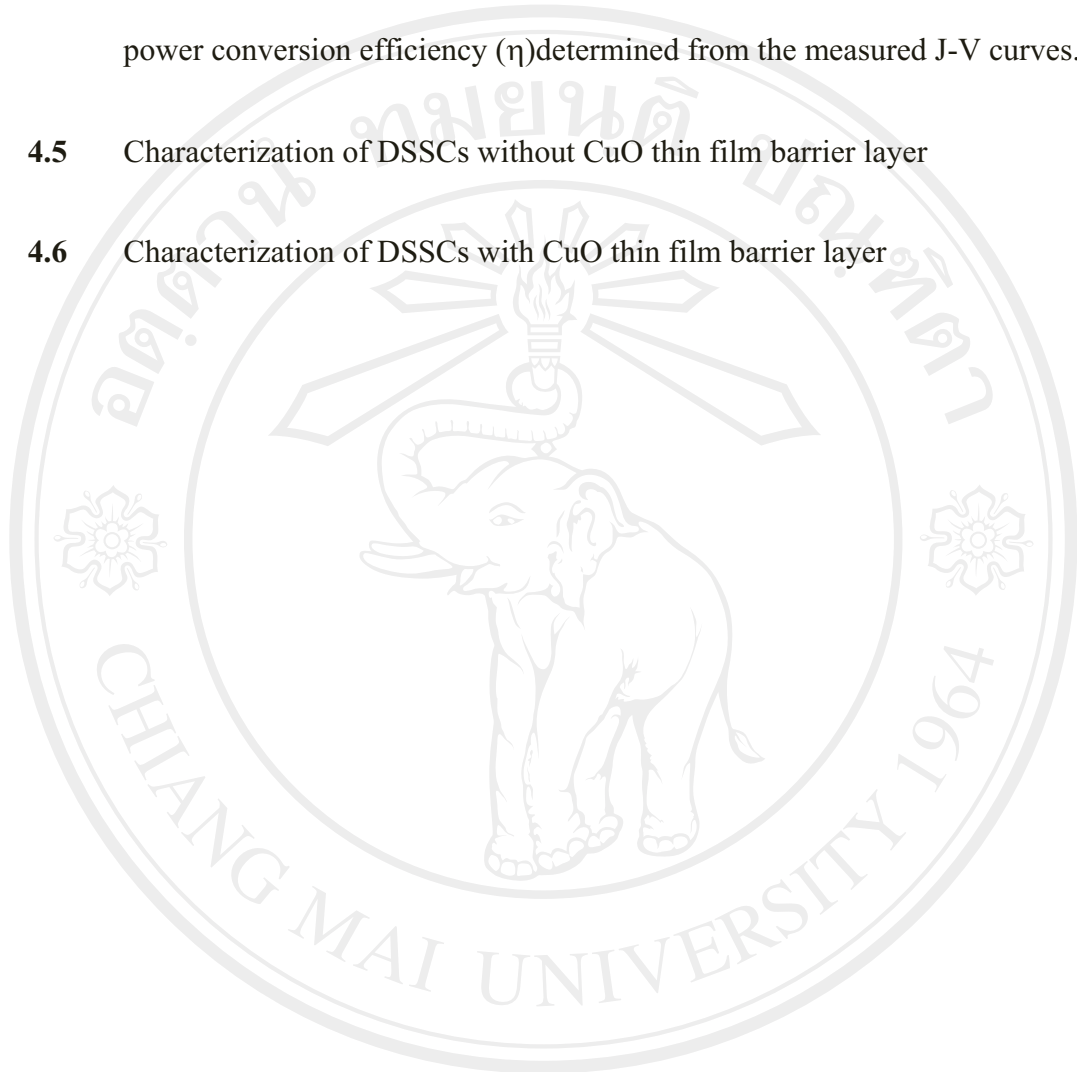
4.3 Preparation of DSSCs	70
4.3.1 ZnO as n-type photoelectrode	71
4.3.2 Standard photoelectrode for ZnO DSSCs	74
4.3.3 Sputtering of ZnO passivating layer for photoelectrode	74
4.3.4 CuO barrier layer photoelectrode	75
4.3.5 Platinum counterelectrode	76
4.3.6 CuO counterelectrode	77
4.3.7 Dye-sensitized solution	77
4.3.8 DSSCs construction	79
4.4 Result of CuO nanostructure in DSSCs	80
4.4.1 Characterization of photoelectrode	80
4.4.2 CuO nanostructure as photoelectrode and counterelectrode	83
4.4.3 CuO as p-n junction DSSCs	84
4.4.4 Effect of barrier layer on photoelectrochemical characteristics	86
4.4.5 The effect of ZnO passivating layer by sputtering ZnO on FTO in DSSCs	88
4.4.6 Impedance result of DSSCs	91

Chapter 5 Conclusions	91
5.1 Preparation of CuO nanostructure	91
5.1.1 Preparation of CuO nanowires on copper plate and copper powder	91
5.1.2 Preparation of CuO thin films on alumina substrate	91
5.2 CuO nanowires for ethanol sensor application	92
5.3 CuO nanostructure for DSSCs application	92
5.3.1 CuO nanostructure as photoelectrode and counterelectrode in ZnO DSSCs application	92
5.3.2 CuO nanostructure as barrier layer of photoelectrode in ZnO DSSCs application	93
5.3.3 ZnO passivating layer with CuO thin films as barrier layer of photoelectrode in ZnO DSSCs application	94
5.4 Suggestion and future works	95
References	97
Appendices	101
Appendix A	102
Appendix B	107
Appendix C	110
Curriculum vitae	123

LIST OF TABLES

Table	Page
1.1 List of the general properties CuO.	5
1.2 List of the general properties of ZnO.	8
2.1 Element content of CuO nanowires	24
2.2 Element content of CuO layer	24
2.3 Element content of Cu ₂ O layer	25
2.4 Show the amount of CuO nanowires per 10 μm^2 and diameter of the nanowires	26
2.5 Element content of CuO thin films on alumina substrate	37
3.1 The ethanol sensing properties of a CuO nanowire sensor at an ethanol concentration of 1000 ppm, and a working temperature of 200-280°C.	50
4.1 Photovoltaic performances of all the DSSCs with and without passivating layer based on TiO ₂ electrode	65
4.2 Preparation of photoelectrode	75
4.3 Summary of the photoelectrochemical parameters such as J_{SC} , V_{OC} , FF and the overall photoconversion efficiency (η) determined from the measured J-V curves in figure 4.21.	84

- 4.4 Summary of the photoelectrochemical parameters such as short current density (J_{sc}), open circuit voltage (V_{oc}), fill factor (FF) and the overall power conversion efficiency (η) determined from the measured J-V curves. 86
- 4.5 Characterization of DSSCs without CuO thin film barrier layer 89
- 4.6 Characterization of DSSCs with CuO thin film barrier layer 89



ลิขสิทธิ์มหาวิทยาลัยเชียงใหม่
Copyright© by Chiang Mai University
All rights reserved

LIST OF FIGURES

Figure	Page
1.1 The relation of dimensionality and density of state.	2
1.2 Monoclinic crystal structure of CuO, Oxygen atoms are shown as blue spheres, copper atoms as red spheres.	5
1.3 (a) the hexagonal wurtzite structure of ZnO, oxygen atoms are shown as large spheres, zinc atoms as smaller spheres and (b) one unit cell of ZnO structure.	7
2.1 SEM images of CuO nanowires prepared by thermal evaporation at various temperatures: (a) 300, (b) 400, (c) 500, (d) 600, (e) 750 and (f) 800°C.	11
2.2 SEM micrographs of CuO nanowires prepared by annealing copper strips for 4 hr under oxygen atmosphere at different temperatures: (a) 500, (b) 600, (c) 700 and (d) 800°C.	12
2.3 (a) TEM and (b) electron diffraction pattern of the as-prepared CuO nanoparticles.	13
2.4 TEM image of the CuO nanowhiskers.	14
2.5 TEM images of the as-prepared CuO nanorods. (a) Morphologies of the as-prepared CuO nanorods. (b) Morphology of the as-prepared single CuO nanorod.	15
2.6 TEM micrograph image of the CuO particles ($\times 150,000$).	16

2.7	The morphologies of the oxide scales formed on Cu foils at: (a) 300°C, showing round oxide grains, (b) 400, (c) 500, (d) 600, (e) 700°C, showing nanowires with different density, size and shape and (f) 800°C, showing oxide crystals.	17
2.8	FE-SEM top view images of thermal oxidation reaction of copper plate at (a) 300, (b) 400, (c) 500, (d) 600, (e) 700 and (f) 800°C in normal atmosphere.	21
2.9	FE-SEM cross-section image of thermal oxidation reaction of copper plate at 600°C.	22
2.10	EDS spectrum selection of CuO nanowires.	23
2.11	EDS spectrum of CuO nanowires.	23
2.12	EDS spectrum selection of CuO layer.	24
2.13	EDS spectrum of CuO layer.	24
2.14	EDS spectrum selection of Cu ₂ O layer.	25
2.15	EDS spectrum of Cu ₂ O layer.	25
2.16	Oxidation reaction process of copper plate.	26
2.17	TEM Bright field image of CuO nanowires (a) projection at 0° and (b) projection at 76°.	27
2.18	(a) bright field image of CuO nanowires (b) SADP of CuO nanowire at line A (c) SADP of CuO nanowire at line B.	27
2.19	Raman shift of CuO nanowires with difference oxidation temperature.	29
2.20	FE-SEM top view images of CuO nanowires on copper powder.	30
2.21	Model of the metal-oxide nucleation for (a) non-reactive and, (b) reactive nucleation and (c) plot of ΔG_N as a function of radius.	31

2.22	Four steps of metal-oxide nanowire growth mechanism, Step 1 - oxygen adsorption, Step 2 - surface oxidization to form nuclei, Step 3 - nuclei arrangement and finally, Step 4 - nanowire formation.	32
2.23	FE-SEM top view images of thermal oxidation reaction of copper thin films at (a) not anneal (b) 300°C for 48 hr, (c) 400°C for 48 hr, (d) 500°C for 48 hr, (e) 600°C for 48 hr, (f) 700°C for 48 hr, (g) 800°C for 48 hr and (h) 900°C for 12 hr.	35
2.24	FE-SEM cross-sections of CuO thin films.	36
2.25	EDS spectrum of CuO thin films.	36
2.26	XRD spectrum of CuO thin films.	38
2.27	Raman peaks of annealed copper thin films on alumina.	38
3.1	(a) Sensor structure and (b) sensing temperature as a function of heater power.	41
3.2	Dynamic gas sensing response of CuO nanowires sensors toward CO and NO ₂ at heater powers of 300 and 400 mW: (a) CO at 300 mW, (b) NO ₂ at 300 mW, (c) CO at 400 mW, and (b) NO ₂ at 400 mW.	41
3.3	Gas sensing transient of the CuO nanowires upon exposure to 5 ppm NO ₂ at 200, 300, and 400°C.	42
3.4	Gas sensing transient to the emissions from a: (a) gasoline engine, 300 mW, (b) diesel engine, 300 mW, (c) gasoline engine, 400 mW, (d) diesel engine, 400 mW.	42
3.5	Conduct-metric response curves to 50 ppm NO ₂ of gas sensors made of CuO particles (a) and plates (b) at different temperatures.	43

- 3.6** Curves of R_{sensor} to 50 ppm NO_2 for gas sensors made of (a) CuO particles and (b) plates at temperature from 100 to 400°C. 44
- 3.7** Typical response curves of gas sensors made of (a) CuO particles and (b) plates to NO_2 with different concentrations at 200°C. 44
- 3.8** Typical response curves of gas sensors with (a) CuO particles and (b) plates to alcohol with different concentrations at 350 °C. 45
- 3.9** Schematic diagram of a sensor fabricated from CuO nanowires and a layer of CuO. 46
- 3.10** Schematic diagram of ethanol sensing simulation. 47
- 3.11** The typical resistance change of an ethanol sensor based on CuO nanostructure. 47
- 3.12** The response and recovery curves of a CuO nanowires sensor at an ethanol concentration of 1000 ppm, working temperature of 200-280°C. 49
- 3.13** The response and the recovery curves of the CuO nanowires sensor at ethanol concentration of 100-1000 ppm and working temperature of 240°C. 49
- 3.14** Log–log plot of gas response and ethanol concentration for CuO nanowires 51
- 4.1** (a) Schematic illustration of the dye-sensitized photovoltaic cell [ITO/TiO₂/dye/E/CuO/Cu], in which p-CuO semiconductor nanorods are used. (b) Schematic energy level diagram showing the band structure alignment and photoinduced charge separation in the photovoltaic cell in (the energy level positions are approximate). 54

- 4.2** Current (I)–voltage (V) characteristics of the dye-sensitized solar cell of the type [ITO/TiO₂/dye/E/CuO/Cu] in the presence and absence of light, where the p-CuO nanorods act as a hole-conducting medium. Inset shows I–V curves for the dye-sensitized solar cell of the type [ITO/TiO₂/dye/E/Pt/ITO]. 55
- 4.3** I–V curves of (a) a dye-sensitized solar cell of the type [ITO/TiO₂/dye/E1/CuO(nanoflake)/Cu] in the presence and absence of light, where the CuO film (prepared at pH 11.8, 90°C, 80 h) acts as a hole transport medium and (b) a reference solar cell [ITO/TiO₂/dye/E1/Pt]. 56
- 4.4** Schematic diagram of SC-SEP PEC cell. 57
- 4.5** Schematic diagram illustrating the energy levels of SnO₂, NiO and the ground and excited energy levels of the Ru-dye. 59
- 4.6** A schematic presentation of electron transfer process for (a) TiO₂/dye, (b) TiO₂/MgO/dye; (a) absorption of light by the dye, (b) injection of excited electron of dye in to the CB of TiO₂, (c and d) regeneration of dye (back reactions). 60
- 4.7** I–V characteristics of p-DSCs using CuO electrodes dyed with four different dyes and an undyed CuO electrode. Irradiation intensity was 100mW/cm². 62
- 4.8** IPCE of p-DSCs using CuO electrodes dyed with four different dyes and an undyed CuO electrode. Inset: Absorption spectra of each dyed and undyed nanoporous CuO electrode. CuO film thickness is 0.34, 0.41, 62

0.52, 0.42 and 0.36 m for Fast Green FCF dye, NK-3628, NK-2612, N3 and without dye.

- 4.9** Energy diagram of the dyes and CuO. 63
- 4.10** schematic diagrams of dye-sensitized solar cells with TiO₂ passivating layer. 64
- 4.11** J-V characteristics for the DSSCs based on nanoporous TiO₂ electrodes (a) without passivating layer and with passivating layer of sputtering pressure (b) 0.1 Pa, (c) 1.0 Pa and (d) 2.0 Pa. 64
- 4.12** Schematic energy diagram for a dye-sensitized solar cell. 66
- 4.13** J-V curve of a solar cell under illumination, displaying the current density and voltage J_{\max} and V_{\max} , respectively, at maximum power. 67
- 4.14** Equivalent circuit for a single junction solar cell. The photogenerated current J_{SC} shows in the inverse direction of the diode. Shunt resistance R_{sh} and series resistance R_{S} are important for the fill factor. Ideally, series resistance should be low and shunt resistance should be high. 68
- 4.15** Schematic diagram of DSSC structures with different photoelectrodes – counterelectrodes for (a) ZnO – CuO nanostructure, (b) ZnO – platinum, and (c) ZnO/CuO nanostructure – platinum. 70
- 4.16** Energy band diagrams of (a) intrinsic (b) n-type semiconductor (c) p-type semiconductor in vacuum. 72
- 4.17** Band positions of several semiconductors in contact with aqueous electrolyte at pH 1. 72
- 4.18** Structural formula of eosin-Y. 79

- 4.19** FE-SEM images of photoelectrodes: (a) ZnO powder/CuO thin film, (b) ZnO powder/CuO powder, (c) ZnO powder/CuO nanowires and (d) ZnO powder, (e), (f), (g) and (h) showed cross-section Fe-SEM images of ZnO powder/CuO thin film, ZnO powder/CuO powder, ZnO powder/CuO nanowires and ZnO powder, respectively. 80
- 4.20** This figure showed XRD pattern of (1) ZnO, (2) ZnO/CuO powder, (3) ZnO/CuO nanowire, and (4) ZnO/CuO thin film on FTO glass substrates. 81
- 4.21** SEM images of ZnO passivating layer with sputtering time of (a) 5 minute, (b) 10 minute, (c) 20 minute and (d) 40 minute. 82
- 4.22** Cross-section SEM images of ZnO passivating layer by sputtering time of (a) 5 minute, (b) 10 minute, (c) 20 minute and (d) 40 minute. 82
- 4.23** J-V characteristics of ZnO DSSCs with different photoelectrodes-counter-electrodes (1) ZnO/CuO nanowire-Pt, (2) ZnO/CuO powder-Pt, (3) ZnO-Pt, (4) ZnO-CuO nanowire and (5) ZnO-CuO powder. 84
- 4.24** Measured J-V characteristic of ZnO DSSCs with ZnO/CuO layer as a photoelectrode. 85
- 4.25** Schematic energy level diagram of (a) ZnO-Pt and (b) ZnO/CuO-Pt (p-n junction photoelectrode). 88
- 4.26** J-V characteristic curve of DSSCs. 89
- 4.27** The relationship of DSSCs with and without CuO thin films as a barrier layer. 90
- A.1** Preparation flow chart of ZnO target 102

A.2	Preparation flow chart for synthesis ZnO nanobelts and nanowires by RF sputtering technique	103
A.3	Preparation flow chart for synthesis ZnO tetrapods by thermal oxidation reaction technique	104
A.4	Ethanol sensing test based on ZnO tetrapods and Pt impregnated ZnO tetrapods	105
A.5	Preparation flow chart of DSSC based ZnO	106
B.1	Schematic diagram of the shape of heterogeneous nucleation on substrate	107

ABBREVIATIONS AND SYMBOLS

RF	radio frequency
P_N	nucleation probability
r^*	critical radius
γ_f	surface energy of film
γ_s	surface energy of substrate
γ_i	surface energy of interface between substrate and film
V_M	system volume
R	gas constant
Φ	surface to volume ratio
$DSSC$	dye-sensitized solar cell
k_B	Boltzman constant
J_{max}	maximum circuit current density
V_{max}	maximum circuit voltage
FF	fill factor
J_{sc}	short circuit current density
V_{oc}	open circuit voltage
$LUMO$	lowest unoccupied molecular orbital
$HOMO$	highest occupied molecular orbital
h	Planck constant
R_s	total series resistance
R_{sh}	shunt resistance
C_i	concentration
ΔG	Gibb free energy
V	voltage
P_{in}	input power
P_{max}	maximum power